

A novel finite-volume TVD scheme to overcome non-realizability problem in quadrature-based moment methods

*Original*

A novel finite-volume TVD scheme to overcome non-realizability problem in quadrature-based moment methods / Shiea, Mohsen; Buffo, Antonio; Vanni, Marco; Marchisio, Daniele L.. - In: JOURNAL OF COMPUTATIONAL PHYSICS. - ISSN 0021-9991. - 409:(2020), p. 109337. [10.1016/j.jcp.2020.109337]

*Availability:*

This version is available at: 11583/2797743 since: 2020-02-26T11:17:15Z

*Publisher:*

Elsevier

*Published*

DOI:10.1016/j.jcp.2020.109337

*Terms of use:*

This article is made available under terms and conditions as specified in the corresponding bibliographic description in the repository

*Publisher copyright*

(Article begins on next page)

# A novel finite-volume TVD scheme to overcome non-realizability problem in quadrature-based moment methods

Mohsen Shiea<sup>a</sup>, Antonio Buffo<sup>a,\*</sup>, Marco Vanni<sup>a</sup>, Daniele L. Marchisio<sup>a</sup>

<sup>a</sup>*Dipartimento di Scienza Applicata e Tecnologia, Politecnico di Torino, Corso Duca degli Abruzzi 24, 10129 Torino, Italy*

---

## Abstract

A new finite-volume total variation diminishing (TVD) scheme is proposed for the solution of moment transport equations in quadrature-based moment methods (QBMM). The proposed scheme is capable of preserving important properties of the moments, such as realizability and boundedness. The idea behind the approach is to limit the flux of all the moments at each cell face with the same limiter value. The proposed numerical technique was eventually compared with other realizable schemes developed for the moment transport equations, showing that the method is able to keep the moments realizable and bounded at the same time.

*Keywords:* Quadrature-based moment methods (QBMM); Moment realizability; Moment boundedness; Population balance equation (PBE); High-resolution scheme; Finite-volume method.

---

## 1. Introduction

The evolution in space and time of a population of disperse elements (e.g., droplets, bubbles or particles moving in a continuous fluid) can be described by using an Eulerian approach through the solution of a generalized

---

\*Corresponding author; current mailing address: Dipartimento di Scienza Applicata e Tecnologia, Politecnico di Torino, Corso Duca degli Abruzzi 24, 10129 Torino, Italy; email: antonio.buffo@polito.it; tel.: +390110904758.

5 population balance equation (GPBE). It is an integro-differential equation  
 6 written in terms of a number density function (NDF) representing, at every  
 7 point of the physical space, the number of elements that have a particular  
 8 state belonging to the so-called phase space, i.e. the space of the properties  
 9 required to characterize the system under investigation (e.g. element size, ve-  
 10 locity, chemical composition, temperature). The Quadrature-Based Moment  
 11 Methods (QBMM) are proved to be efficient in solving the GPBE, where the  
 12 transport equations for some moments of the underlying NDF are solved in-  
 13 stead of the GPBE [1]. These methods are based on the assumption that the  
 14 underlying NDF has the form of a multi-dimensional summation of weighted  
 15 kernel density functions (KDF) centered on the quadrature abscissas, where  
 16 the quadrature weights and abscissas can be retrieved from the moments by  
 17 means of the so-called inversion algorithms (such as the Product-Difference  
 18 (PD) [2] and the Chebyshev [3] algorithms). In most cases, the KDF is a  
 19 Dirac delta function, especially when a continuous reconstruction of the NDF  
 20 is not necessary. While these methods are efficient and promising, especially  
 21 when coupled with Computational Fluid Dynamics (CFD) codes, their prac-  
 22 tical use encounters inherent difficulties to cope with. One major issue is  
 23 the realizability or consistency of the transported moment set, meaning that  
 24 there must exist an underlying number density function (NDF) corresponding  
 25 to the transported moments. Confining the discussion to the finite-volume  
 26 method, the most common cause of the non-realizability (also known as nu-  
 27 merical moment corruption) lies in the spatial discretization of the transport  
 28 term of the moment equation, when high-order spatial discretization schemes  
 29 are used. This problem is often related to the convective term, as in many

cases the governing equations have a hyperbolic form. Desjardins et al. [4] demonstrated that the 1<sup>st</sup>-order scheme guarantees the realizability of the moments, provided the CFL condition is respected. However, this scheme results in highly diffusive solutions, leading sometimes to unacceptable predictions, hence the necessity of adopting high-order schemes. On the other hand, employing high-order finite-volume schemes for independent transport of the moments may cause non-realizability issues [5]. Therefore, the development of a realizable high-order scheme for the solution of moment transport equations is crucial. In this regard, Vikas and co-workers [6] presented the so-called realizable quasi-high-order schemes, based on the evaluation of the moment fluxes at the cell faces using the interpolated abscissas and weights of the quadrature. With this method, the quadrature interpolation is performed by applying 1<sup>st</sup>-order scheme to the quadrature abscissas and high-order schemes to the quadrature weights. This approach produces less diffusive solutions and guarantees the realizability of the transported moments, provided a criterion on the time step is respected. However, no analysis was conducted on the boundedness property of this approach, which can not be ignored since unbounded predictions are not physically allowed [7]. Kah et al. [8] formulated a 2<sup>nd</sup>-order kinetic scheme that makes use of the canonical moments to transport the moments indirectly while maintaining them in the moment space. However, the application of their method to simulations with more than four moments involves difficult algebra [9]. Recently, Laurent and co-workers [9] developed a similar approach based on reconstructing the coefficients  $\zeta_k$  (for its definition refer to [9]) instead of the canonical moments. However, their original  $\zeta_k$  reconstruction based scheme

55 cannot be applied easily to the unstructured grids and therefore they sug-  
56 gested a simplified version of this scheme that involves division of the cells  
57 into three parts as proposed by Berthon [10].

58 The present work introduces a new technique, called equal-limiter scheme,  
59 to overcome the non-realizability problem when 2<sup>nd</sup>-order TVD (Total Vari-  
60 ation Diminishing) schemes are applied to the moment transport equations.  
61 The technique is based on using an equal limiter given by the flux-limiter  
62 function for all the moments, and it will be shown that it is effective to  
63 avoid non-realizable set of moments. Moreover, its application to three-  
64 dimensional unstructured grids is straightforward. The paper is organized as  
65 follows. First, it will be proved that, in a one-dimensional Riemann problem,  
66 the concept of equal-limiter emerges naturally if no source term is included in  
67 the moment transport equations. Next, the importance of using an identical  
68 limiter given by the limiter function for all the moments will be clarified in  
69 a general case by solving local Riemann problem at each cell face and the  
70 role of the time step in maintaining the realizability of the moments will be  
71 explained. Moreover, the paper shows how this technique can be applied to  
72 CFD codes, without any assumption on velocity field or type of mesh grid. In  
73 the final part, a comparison between different techniques will be performed  
74 by solving moment transport equations in some one- and two-dimensional  
75 test cases.

## 2. TVD scheme for moment transport equation

### 2.1. Moment transport equation

As previously mentioned, QBMM deal with the solution of the transport equations written in terms of the moments of the NDF, instead of the GPBE itself. The NDF is a complex multi-dimensional functional that depends on the so-called external coordinates, i.e. the position of the elements in the physical space and time, and on the internal coordinates, which are the generic properties associated to each element of the population, such as size, velocity, chemical composition or temperature. When the internal coordinates do not include the velocity of the elements of the disperse phase, the resulting transport equation for the NDF is called Population Balance Equation (PBE) [1]. Although it is possible to apply the proposed numerical scheme to the transport equation for a multivariate set of moments, let us consider a univariate PBE with the size of the elements of the disperse phase,  $L$ , as the internal coordinate, for the sake of simplicity and clarity. In this case, the PBE can be written as follows [11]:

$$\frac{\partial f}{\partial t} + \frac{\partial(\mathbf{U}f)}{\partial \mathbf{x}} + \frac{\partial(\dot{L}f)}{\partial L} = h \quad (1)$$

where  $f \equiv f(L, \mathbf{x}, t)$  denotes the NDF. In addition,  $\mathbf{U} \equiv \mathbf{U}(\mathbf{x}, t)$  is the velocity of the disperse phase,  $\dot{L}$  represents the continuous rate of change in the size of elements due to the continuous processes (e.g. mass transfer driven growth) and  $h$  introduces the contribution of the discrete events (e.g. aggregation/breakage) into the PBE. It is worth remarking that the velocity of the disperse phase appearing in Eq. (1) does not depend on the size of

the elements: such approximation has been made to simplify the following discussion and it is not a limitation of the proposed approach.

By definition, the  $k^{\text{th}}$ -order moment of  $f$  with respect to  $L$  is:

$$M^k(\mathbf{x}, t) = \int_0^\infty f(L, \mathbf{x}, t) L^k dL \quad (2)$$

The importance of the moments lies in the fact that lower-order moments are associated to various integral properties of the population. For instance, in this case the 3<sup>rd</sup>-order moment with respect to  $L$  is proportional to the volume fraction of the disperse phase. The above definition can be used to derive moment transport equations from Eq. (1). For the sake of simplicity, from now on we assume a one-dimensional case where the velocity is constant ( $u$ ) and the contribution of the continuous processes is negligible ( $\dot{L} = 0$ ). The transport equation for the  $k^{\text{th}}$ -order moment reduces to the following partial differential equation:

$$\frac{\partial M^k}{\partial t} + u \frac{\partial M^k}{\partial x} = \bar{h}^k \quad (3)$$

where  $\bar{h}^k$  is the source term changing the  $k^{\text{th}}$ -order moment due to the discrete events. Generally, this source term is a complex multi-dimensional integral which depends on the NDF itself. QBMM employ the so-called quadrature approximation to express the functional form of the NDF. If we consider only one internal coordinate, it is possible to write a generic integral in the following way and therefore close the moment transport equations:

$$\int_{\Omega_L} f(L) g(L) dL = \sum_{\alpha=1}^N w_\alpha g(L_\alpha) \quad (4)$$

where  $w_\alpha$  and  $L_\alpha$  are the weights and abscissas of the  $N$ -node quadrature formula. This means that the NDF is approximated as a summation of delta

118 functions centered on quadrature abscissas:

$$f(L) = \sum_{\alpha=1}^N w_{\alpha} \delta(L - L_{\alpha}) \quad (5)$$

119 This method is called Quadrature Method of Moments (QMOM) and it is  
120 designed to solve univariate PBE [12]. The weights and abscissas are deter-  
121 mined from the transported moments by employing an inversion algorithm  
122 (such as PD or Chebyshev algorithms), provided the set of moments is re-  
123 alizable. This is usually referred as the moment problem [13]: in particular,  
124 when the support of the NDF is  $\Omega_L = ]0, +\infty[$  as in this case, it is called  
125 finite Stieltjes moment problem. When the support of the NDF is different,  
126 i.e.  $\Omega_L = ]-\infty, +\infty[$  or  $\Omega_L = ]0, 1[$ , we refer to finite Hamburger and finite  
127 Hausdorff moment problems respectively. These three different supports re-  
128 sult in different constraints on the transported set of moments to ensure  
129 its realizability [13, 14]. However, the non-realizability problem is common  
130 to all these cases and poses the main challenge in practical applications of  
131 QMOM. In the finite-volume method, this can happen particularly during  
132 the interpolation of the moments on to the faces to calculate the flux of the  
133 moments through faces if high-resolution TVD schemes are employed.

## 134 2.2. Finite-Volume Method

135 As mentioned before, the present study focuses on the non-realizability  
136 issue in the context of the finite-volume method. The general formulation  
137 of the finite-volume method can be found in the specialized literature [15,  
138 16], and therefore is omitted here. Let a single-stage explicit method be  
139 adopted to march in time and the source terms be handled using fractional-  
140 step approach [15]. In this way, the finite-volume method transforms Eq. (3)



141 into the following discretized form written for the generic cell  $i$  of size  $\Delta x$  in  
 142 the spatial domain:

$$M_i^{k*} = M_i^k - \frac{\Delta t}{\Delta x} (F_{i+1/2}^k - F_{i-1/2}^k) \quad (6)$$

$$(M_i^k)^{n+1} = M_i^{k*} - \Delta t \bar{h}_i^k \quad (7)$$

143 where  $M_i^k$ ,  $M_i^{k*}$  and  $(M_i^k)^{n+1}$  refer to, respectively, the moment value at the  
 144 current time ( $t_n$ ), the intermediate value of the fractional-step approach and  
 145 the moment value at the new time ( $t_{n+1}$ ) after a time step of  $\Delta t$ . Further-  
 146 more,  $F_{i-1/2}^k$  and  $F_{i+1/2}^k$  denote the numerical flux along the left and right  
 147 faces of the cell  $i$  respectively, each depends on the neighboring cell values at  
 148 time  $t_n$  according to the selected numerical flux function. From now on, the  
 149 primary focus of the work will be on Eq. (6), particularly the calculation of  
 150 the flux of the moments at the faces. The effect of the source term will be  
 151 clarified afterwards.

152 It is desirable to calculate the fluxes using high-resolution schemes, which  
 153 are on the basis of slope-limiter methods. These methods use a high-order  
 154 scheme where the solution is smooth enough, otherwise they switch to a low-  
 155 order one to prevent non-physical oscillations in the numerical solution [15].  
 156 In this way, the solution exhibits higher order of accuracy, comparing to 1<sup>st</sup>-  
 157 order solution, without losing the boundedness. Using Lax-Wendroff as the  
 158 high-order scheme and upwind as the low-order one will form the so-called  
 159 flux-limiter methods with the following numerical flux functions [15]:

$$F_{i-1/2}^k = u^- M_i^k + u^+ M_{i-1}^k + \frac{1}{2} |u| \left( 1 - \frac{|u| \Delta t}{\Delta x} \right) \phi(\theta_{i-1/2}^k) \Delta M_{i-1/2}^k \quad (8)$$

$$F_{i+1/2}^k = u^- M_{i+1}^k + u^+ M_i^k + \frac{1}{2} |u| \left( 1 - \frac{|u| \Delta t}{\Delta x} \right) \phi(\theta_{i+1/2}^k) \Delta M_{i+1/2}^k \quad (9)$$

160 where

$$u^+ = \frac{1}{2}(u + |u|) \quad \text{and} \quad u^- = \frac{1}{2}(u - |u|) \quad (10)$$

161 In addition,  $\Delta M_{i-1/2}^k$  and  $\Delta M_{i+1/2}^k$  are respectively the jumps across the left  
162 and right faces, defined following the below convention:

$$\Delta M_{i-1/2}^k = M_i^k - M_{i-1}^k \quad (11)$$

163 The flux-limiter  $\phi$  is a function of the smoothness of  $M^k$  at the face  $(\theta_{i\pm 1/2}^k)$ .

164 The smoothness is commonly defined as follows [15]:

$$\theta_{i-1/2}^k = \frac{\Delta M_{I-1/2}^k}{\Delta M_{i-1/2}^k} \quad \text{with} \quad I = \begin{cases} i-1 & \text{if } u \geq 0 \\ i+1 & \text{if } u < 0 \end{cases} \quad (12)$$

165 A variety of flux-limiter functions are available in the literature such as min-  
166 mod [17] and van Leer [18].

167 Substituting the numerical fluxes in Eq. (6) yields the following dis-  
168 cretized equation:

$$M_i^{k*} = M_i^k - \frac{\Delta t}{\Delta x} u^+ (M_i^k - M_{i-1}^k) - \frac{\Delta t}{\Delta x} u^- (M_{i+1}^k - M_i^k) \\ - \frac{1}{2} \frac{|u| \Delta t}{\Delta x} \left( 1 - \frac{|u| \Delta t}{\Delta x} \right) \left[ \phi(\theta_{i+1/2}^k) \Delta M_{i+1/2}^k - \phi(\theta_{i-1/2}^k) \Delta M_{i-1/2}^k \right] \quad (13)$$

### 169 3. The Concept of Equal-Limiter

170 The flux-limiter methods were developed to address the issue of bound-  
171 edness that occurs in the case of employing high-order schemes to solve hy-  
172 perbolic problems. One would ideally desire to use these methods for the  
173 solution of the moment transport equations, particularly when the 1<sup>st</sup>-order

accuracy is not sufficient to describe the behavior of the system under study. However, in general, the non-realizability problem hinders their direct practice in solving the moments transport equations. In this section, it is shown that this limitation can be overcome by selecting an equal limiter for all the moments.

The starting point is to show that the idea of equal-limiter emerges in the case of employing 2<sup>nd</sup>-order TVD schemes for the pure moment advection with no source term ( $(M_i^k)^{n+1} = M_i^{k*}$ ) in a Riemann problem example. It will be also shown that in this case the moments remain realizable. Then, the discussion will continue to highlight the advantage of employing equal-limiter in a more general context, where the effect of aggregation and breakage will be also taken into account.

The argument begins with rewriting Eq. (13) for the case  $u > 0$  without loss of generality<sup>1</sup>:

$$(M_i^k)^{n+1} = M_i^k - \nu(M_i^k - M_{i-1}^k) - \frac{1}{2}\nu(1-\nu) [\phi(\theta_{i+1/2}^k)\Delta M_{i+1/2}^k - \phi(\theta_{i-1/2}^k)\Delta M_{i-1/2}^k] \quad (14)$$

where  $\nu = u\Delta t/\Delta x$  is the Courant number. The smoothness at the left and right faces are written as follows Eq. (12):

$$\theta_{i-1/2}^k = \frac{M_{i-1}^k - M_{i-2}^k}{M_i^k - M_{i-1}^k} \quad \text{and} \quad \theta_{i+1/2}^k = \frac{M_i^k - M_{i-1}^k}{M_{i+1}^k - M_i^k} \quad (15)$$

Now let us consider a Riemann problem example with the following initial

---

<sup>1</sup>The case  $u < 0$  can be formulated similarly and leads to the same conclusions

191 data:

$$M^k(x, 0) = \overset{\circ}{M}^k = \begin{cases} \overset{\circ}{M}_l^k & \text{if } x < 0 \\ \overset{\circ}{M}_r^k & \text{if } x > 0 \end{cases} \quad (16)$$

192 where  $\overset{\circ}{M}_l^k$  and  $\overset{\circ}{M}_r^k$  are obtained from the initial left and right NDFs,  $\overset{\circ}{f}_l$  and  $\overset{\circ}{f}_r$ ,  
 193 and consequently constitute two realizable sets of moments. It is postulated  
 194 that the numerical solution of the  $k^{\text{th}}$ -order moment at any generic cell  $i$  and  
 195 any time step  $t_n$ , including the zero time, can be expressed as:

$$M_i^k = \overset{\circ}{M}_r^k - a_i^n (\overset{\circ}{M}_r^k - \overset{\circ}{M}_l^k) \quad , \quad 0 \leq a_i^n \leq 1 \quad (17)$$

196 where  $a_i^n$  is a constant that changes with the cell index  $i$  and the time step  
 197 but not due to the moment order or value. In other words, this constant is  
 198 the same for all the moments of a given cell at each time step. It is worth  
 199 mentioning that the initial data (Eq. (16)) corresponds to  $a_i^0 = 1$  for  $x_i < 0$   
 200 and  $a_i^0 = 0$  for  $x_i > 0$ . Next step is to substitute Eq. (17) in Eq. (14), which  
 201 after simplifications yields the following:

$$\begin{aligned} (M_i^k)^{n+1} &= \overset{\circ}{M}_r^k - a_i^n (\overset{\circ}{M}_r^k - \overset{\circ}{M}_l^k) + \nu (a_i^n - a_{i-1}^n) (\overset{\circ}{M}_r^k - \overset{\circ}{M}_l^k) \\ &\quad + \frac{1}{2} \nu (1 - \nu) \left[ \phi \left( \frac{a_i^n - a_{i-1}^n}{a_{i+1}^n - a_i^n} \right) (a_{i+1}^n - a_i^n) \right. \\ &\quad \left. - \phi \left( \frac{a_{i-1}^n - a_{i-2}^n}{a_i^n - a_{i-1}^n} \right) (a_i^n - a_{i-1}^n) \right] (\overset{\circ}{M}_r^k - \overset{\circ}{M}_l^k) \\ &= \overset{\circ}{M}_r^k - a_i^{n+1} (\overset{\circ}{M}_r^k - \overset{\circ}{M}_l^k) \end{aligned} \quad (18)$$

202 and  $a_i^{n+1}$  collects several coefficients that do not depend on the moment

203 values:

$$\begin{aligned}
a_i^{n+1} = & a_i^n - \nu(a_i^n - a_{i-1}^n) \\
& - \frac{1}{2}\nu(1 - \nu) \left[ \phi \left( \frac{a_i^n - a_{i-1}^n}{a_{i+1}^n - a_i^n} \right) (a_{i+1}^n - a_i^n) \right. \\
& \left. - \phi \left( \frac{a_{i-1}^n - a_{i-2}^n}{a_i^n - a_{i-1}^n} \right) (a_i^n - a_{i-1}^n) \right]
\end{aligned} \tag{19}$$

204 Equation (19) has the same structure of Eq. (14), therefore, it appears that  
205  $a_i^n$  is the solution of an advection equation for the variable  $a$  obtained by the  
206 2<sup>nd</sup>-order TVD finite-volume scheme. As a consequence, it is guaranteed that  
207  $a_i^{n+1}$  remains bounded to the values of the previous time step, i.e. between  
208 0 and 1. Now it can be concluded that the postulated solution at time step  
209  $t_n$  is also valid at the next time step  $t_{n+1}$ :

$$(M_i^k)^{n+1} = \overset{\circ}{M}_r^k - a_i^{n+1}(\overset{\circ}{M}_r^k - \overset{\circ}{M}_l^k), \quad 0 \leq a_i^{n+1} \leq 1 \tag{20}$$

210 As mentioned before, the initial data (Eq. (16)) can be expressed by Eq. (17),  
211 therefore, the postulated solution is indeed the solution of Eq. (14) at any  
212 time step with the initial data defined by Eq. (16). Moreover, it can be  
213 proved that the solution guarantees the realizability of the moments at any  
214 time step if the initial set is realizable. To proceed with the proof, the  
215 following notation is used for representing the set of moments:

$$\mathbf{W} = [M^0 \ M^1 \ \dots \ M^{2N-1}]^T \tag{21}$$

216 It is worth reiterating that  $N$  is the number of quadrature nodes. The set of  
217 moments can be defined as follows:

$$\mathbf{W} = \int_0^\infty f(L)\mathbf{q}(L)dL \tag{22}$$

218 where  $\mathbf{q}(L) = [L^0 \ L^1 \ \dots \ L^{2N-1}]^T$ .

219 Equation (20) can be written for the set of moments by using the notation  
220 introduced in Eq. (21):

$$\mathbf{W}_i^{n+1} = \mathbf{W}_r - a_i^{n+1}(\mathbf{W}_r - \mathbf{W}_l) \quad (23)$$

221 It should be emphasized that Eq. (23) is derived based on the fact that  $a_i^{n+1}$   
222 is identical for all the moments. The proof follows by substituting Eq. (22)  
223 in Eq. (23) and performing some manipulations:

$$\int_0^\infty f_i^{n+1} \mathbf{q}(L) dL = \int_0^\infty [(1 - a_i^{n+1}) \overset{\circ}{f}_r + a_i^{n+1} \overset{\circ}{f}_l] \mathbf{q}(L) dL \quad (24)$$

224 OR

$$f_i^{n+1} = (1 - a_i^{n+1}) \overset{\circ}{f}_r + a_i^{n+1} \overset{\circ}{f}_l \quad (25)$$

225 The above equation guarantees the non-negativity of the  $f_i^{n+1}$  because both  
226  $\overset{\circ}{f}_r$  and  $\overset{\circ}{f}_l$  are defined to be non-negative NDFs and  $0 \leq a_i^{n+1} \leq 1$ . Conse-  
227 quently, the moment set of cell  $i$  at time step  $t_{n+1}$  is realizable, see [4].

228 Returning back to the equal-limiter concept, it was previously highlighted  
229 that an identical  $a_i^{n+1}$  for all the moments is essential to keep the moment  
230 set realizable in a Riemann problem example. The identical  $a_i^{n+1}$  originates,  
231 in turn, from the equal limiters calculated at the left and right faces (i.e.,  
232 Eq. (18)):

$$\phi(\theta_{i-1/2}^k) = \phi\left(\frac{a_{i-1}^n - a_{i-2}^n}{a_i^n - a_{i-1}^n}\right) \quad \text{and} \quad \phi(\theta_{i+1/2}^k) = \phi\left(\frac{a_i^n - a_{i-1}^n}{a_{i+1}^n - a_i^n}\right). \quad (26)$$

233 When source terms are present, the limiters are not generally identical for  
234 all the moments, because in this case the smoothness of the moments may

change differently and this may cause the non-realizability of the transported  
moment set. This suggests to find a technique to employ an identical limiter  
in the calculation of the moment fluxes at the faces.

Again Eq. (13) is rewritten for the case of  $u > 0$  (here a local Riemann  
problem is solved at each face of cell  $i$ ):

$$M_i^{k*} = M_i^k - \nu(M_i^k - M_{i-1}^k) - \frac{1}{2}\nu(1-\nu)[\phi(\theta_{i+1/2}^k)\Delta M_{i+1/2}^k - \phi(\theta_{i-1/2}^k)\Delta M_{i-1/2}^k] \quad (27)$$

which can simply be expressed as follows by collecting the terms containing  
the moment of cells  $i-1$ ,  $i$  and  $i+1$ :

$$M_i^{k*} = B_i^k M_{i-1}^k + C_i^k M_i^k - D_i^k M_{i+1}^k \quad (28)$$

with

$$\begin{aligned} B_i^k &= \nu - \frac{1}{2}\nu(1-\nu)\phi(\theta_{i-1/2}^k) \\ C_i^k &= 1 - \nu + \frac{1}{2}\nu(1-\nu)[\phi(\theta_{i+1/2}^k) + \phi(\theta_{i-1/2}^k)] \\ D_i^k &= \frac{1}{2}\nu(1-\nu)\phi(\theta_{i+1/2}^k) \end{aligned} \quad (29)$$

Writing Eq. (28) for the set of moments of order  $k = 1, 2, \dots, 2N-1$  yields:

$$\begin{pmatrix} M_i^{0*} \\ M_i^{1*} \\ \vdots \\ M_i^{2N-1*} \end{pmatrix} = \underbrace{\begin{pmatrix} B_i^0 M_{i-1}^0 \\ B_i^1 M_{i-1}^1 \\ \vdots \\ B_i^{2N-1} M_{i-1}^{2N-1} \end{pmatrix}}_{\text{set } i-1} + \underbrace{\begin{pmatrix} C_i^0 M_i^0 \\ C_i^1 M_i^1 \\ \vdots \\ C_i^{2N-1} M_i^{2N-1} \end{pmatrix}}_{\text{set } i} - \underbrace{\begin{pmatrix} D_i^0 M_{i+1}^0 \\ D_i^1 M_{i+1}^1 \\ \vdots \\ D_i^{2N-1} M_{i+1}^{2N-1} \end{pmatrix}}_{\text{set } i+1} \quad (30)$$

244 The three sets of moments in Eq. (30) can easily become non-realizable be-  
 245 cause, in general, the coefficients  $B_i^k$  as well as  $C_i^k$  and  $D_i^k$  might differ from  
 246 one moment to another (belonging to the same moment set) as a consequence  
 247 of unequal limiters. Marchisio and Fox [1] showed that a small change in just  
 248 one moment can make a consistent set of moments non-realizable. On the  
 249 other hand, if identical limiters are selected to estimate the fluxes of all the  
 250 moments at the left and right faces, Eq. (30) can be written as follows:

$$\int_0^\infty f_i^* \mathbf{q}(L) dL = \int_0^\infty (B_i f_{i-1} + C_i f_i - D_i f_{i+1}) \mathbf{q}(L) dL \quad (31)$$

251 OR

$$f_i^* = B_i f_{i-1} + C_i f_i - D_i f_{i+1} \quad (32)$$

252 where  $B_i$  as well as  $C_i$  and  $D_i$  are defined below by choosing an equal limiter  
 253 at the left face,  $\phi(\theta_{i-1/2})$ , and one at the right face,  $\phi(\theta_{i+1/2})$ , for all the  
 254 moments:

$$\begin{aligned} B_i &= \nu - \frac{1}{2}\nu(1-\nu)\phi(\theta_{i-1/2}) \\ C_i &= 1 - \nu + \frac{1}{2}\nu(1-\nu)[\phi(\theta_{i+1/2}) + \phi(\theta_{i-1/2})] \\ D_i &= \frac{1}{2}\nu(1-\nu)\phi(\theta_{i+1/2}) \end{aligned} \quad (33)$$

255 It should be noted that there is still no proof for the moment realizability  
 256 in the case of employing equal limiters when source terms in the moment  
 257 transport equation are present, because the last term in Eq. (32) is negative  
 258 [4] [6]. However, the contribution of the negative term can be kept small  
 259 enough through adjusting the time step since the coefficient  $D_i$  diminishes as  
 260 the time step is reduced to zero. In other words, the non-realizability problem



261 can be prevented by adjusting the time step, whereas it can arise easily  
 262 regardless of the time step if the limiters are calculated independently. One  
 263 should be careful when the moment sets lie on the boundary of the moment  
 264 space. In such case, the underlying number density functions are indeed  
 265 some point distributions, i.e summation of some weighted delta functions.  
 266 Therefore, if the moment sets in Eq. (30) are near or on the boundary of the  
 267 moment space, reduction of the time step cannot resolve the realizability issue  
 268 since the supports of the corresponding underlying number density functions  
 269 in Eq. (32) may hardly match each other. A possible remedy can be adopting  
 270 the 1-D adaptive quadrature technique proposed by Yuan and co-workers [19].  
 271 By this technique, the maximum number of quadrature nodes is selected in  
 272 such a way that the moments required to calculate the quadrature weights  
 273 and abscissas form a set which is located in the interior of the moment space.  
 274 It is noteworthy that the local reduction of the number of quadrature nodes  
 275 is not a problem for the equal-limiter scheme, in contrast to the quasi-high-  
 276 order scheme, since the variables to be interpolated are the moments and not  
 277 the quadrature abscissas and weights.

278 The final point to be addressed is the choice of an equal flux-limiter at  
 279 each face. In fact, the constraint on the boundedness of the solution narrows  
 280 the choice of the equal flux-limiter. As mentioned before, the 2<sup>nd</sup>-order TVD  
 281 schemes have this notable feature of preserving the solution bounded. It is  
 282 extremely useful for the QMOM since the low-order moments are propor-  
 283 tional to physical properties that are bounded in nature, such as mean size,  
 284 surface area or volume fraction. Harten [20] established the sufficient crite-  
 285 ria for a scheme to be TVD, which provide constraints on the flux-limiter

286 functions:

$$\phi(\theta) = 0 \quad \text{if } \theta < 0 \quad \text{and} \quad 0 \leq \phi(\theta) \leq \min(2\theta, 2) \quad \text{if } \theta \geq 0 \quad (34)$$

287 Fig. 1 represents these constraints graphically (shaded area) following the  
 288 work of Sweby [21]. Moreover, it depicts the 2<sup>nd</sup>-order region proposed by  
 289 Sweby [21] (hatched area) within which the flux-limiter functions lie. Two  
 290 such examples are shown by the solid line (minmod limiter [17]) and the  
 291 dashed line (van Leer limiter [18]).

292 The flux-limiter functions in the literature share the common feature of  
 293 being non-decreasing functions of  $\theta$ . Using this feature, it is simple to show  
 294 that the smallest flux-limiter among all the limiters of the moments is an  
 295 obvious choice that guarantees the boundedness of all the moments. The  
 296 flux-limiters calculated independently by a general limiter function at a given  
 297 face,  $e$ , can be represented as  $\phi(\theta_e^k)$  with  $k = 0, 1, \dots, 2N - 1$ . These limiters  
 298 respect the conditions expressed in Eq. (34):

$$\phi(\theta_e^k) = 0 \quad \text{if } \theta_e^k < 0 \quad \text{and} \quad 0 \leq \phi(\theta_e^k) \leq \min(2\theta_e^k, 2) \quad \text{if } \theta_e^k \geq 0 \quad (35)$$

299 Suppose that  $\phi_e^{\min}$  denotes the limiter with the minimum value:

$$\phi_e^{\min} = \phi(\theta_e^m) \leq \phi(\theta_e^k) \quad \text{for } k = 0, 1, \dots, 2N - 1 \quad (36)$$

300 where

$$\theta_e^m \in \{\theta_e^k \mid k \in \{0, 1, \dots, 2N - 1\}\} \quad (37)$$

301 and since the flux-limiter functions are non-decreasing:

$$\theta_e^m \leq \theta_e^k \quad \text{for } k = 0, 1, \dots, 2N - 1 \quad (38)$$

302 On the other hand, the upper boundary of the TVD region shown in Eq. (35),  
 303  $\min(2\theta_e^k, 2)$ , is a non-decreasing function, therefore:

$$\min(2\theta_e^m, 2) \leq \min(2\theta_e^k, 2) \quad \text{for } k = 0, 1, \dots, 2N - 1 \quad (39)$$

304 since  $\phi_e^{\min}$  respects the conditions specified in Eq. (35), it can be concluded  
 305 that:

$$0 \leq \phi_e^{\min} \leq \min(2\theta_e^k, 2) \quad \text{for } k = 0, 1, \dots, 2N - 1 \quad (40)$$

306 in other words,  $\phi_e^{\min}$  falls always in the TVD region specified in Fig. 1 for all  
 307 the moments. As a result, the moments remain bounded using this limiter,  
 308 following the proof given by Harten [20].

309 It should be mentioned that, in general, the minimum limiter can fall  
 310 outside the 2<sup>nd</sup>-order region of Sweby for some moments, hence resulting in  
 311 solutions with accuracy of lower order. Nevertheless, the numerical results  
 312 reported in the next section show remarkable improvements in comparison  
 313 to the 1<sup>st</sup>-order solutions. More importantly, the results indicate a significant  
 314 advantage of the proposed scheme over the realizable high-order scheme of  
 315 Vikas et al. [6] since it is able to produce bounded solutions.

#### 316 4. Application to CFD Codes

317 This section focuses on the application of the equal-limiter scheme to CFD  
 318 codes, which is indeed our ultimate goal of introducing this scheme. For this  
 319 purpose, the following three-dimensional conservative transport equation is  
 320 considered for the  $k^{\text{th}}$ -order moment:

$$\frac{\partial M^k}{\partial t} + \frac{\partial}{\partial \mathbf{x}} \cdot (\mathbf{u} M^k) = 0 \quad (41)$$

321 The source term is not included since the focus is only on the advection of the  
 322 moments. In the context of finite volume methods, Eq. (41) is integrated over  
 323 the volume of each computational cell and then the integral of the convective  
 324 term over the volume of each cell is replaced with the net flux of the moment  
 325 through the faces of that cell (Gauss's theorem). Therefore, the following  
 326 semi-discretized equation is obtained for a generic cell  $i$  [16]:

$$\frac{dM_i^k}{dt} + \frac{1}{\Delta V_i} \sum_e (\mathbf{u}_e \cdot \hat{\mathbf{n}}_e) S_e M_e^k = 0 \quad (42)$$

327 where  $M_e^k$  and  $\mathbf{u}_e$  are the moment of order  $k$  and the velocity at a generic  
 328 face  $e$  of cell  $i$  respectively. In addition,  $\hat{\mathbf{n}}_e$  and  $S_e$  denote respectively the  
 329 outward unit normal vector and the surface area of face  $e$  and  $\Delta V_i$  is the  
 330 volume of the cell  $i$ . The transient term in Eq. (42) is not discretized for the  
 331 reason that becomes clear later. In CFD codes, the flux of the velocity field  
 332 at the cell faces, i.e.  $(\mathbf{u}_e \cdot \hat{\mathbf{n}}_e) S_e$ , is generally known. However, the value of  
 333 the moments at the faces ( $M_e^k$ ) is not available and should be interpolated  
 334 from the values at the centers of neighbouring cells.

335 The implementation of high-resolution TVD schemes in CFD codes is usually  
 336 on the basis of central-difference scheme, of which the anti-diffusive contri-  
 337 bution is limited to prevent oscillations in the solution [22]:

$$M_e^k = \underbrace{M_U^k}_{\text{upwind}} + \phi(\theta_e^k) \underbrace{\lambda_e (M_D^k - M_U^k)}_{\text{anti-diffusive part}} \quad (43)$$

338 where  $M_U^k$  and  $M_D^k$  refer to the values of the moment of order  $k$  at the centers  
 339 of the upwind and downwind cell neighbours of the face  $e$  respectively. The  
 340 selection of the upwind and downwind cells is based on the direction of the  
 341 velocity field at face  $e$ , which is the same for all the moments. In addition,

the coefficient  $\lambda_e$  takes a positive constant value between 0 and 0.5, which depends on the distances between the center of face  $e$  and the centers of the two neighbouring cells. The advantage of employing an identical limiter can be illustrated by rearranging Eq. (43) and writing it for a set of  $2N - 1$  moments as follows:

$$\underbrace{\begin{pmatrix} M_e^0 \\ M_e^1 \\ \vdots \\ M_e^{2N-1} \end{pmatrix}}_{\text{set } e} = \underbrace{\begin{pmatrix} [1 - \lambda_e \phi(\theta_e^0)] M_U^0 \\ [1 - \lambda_e \phi(\theta_e^1)] M_U^1 \\ \vdots \\ [1 - \lambda_e \phi(\theta_e^{2N-1})] M_U^{2N-1} \end{pmatrix}}_{\text{set U}} + \underbrace{\begin{pmatrix} \lambda_e \phi(\theta_e^0) M_D^0 \\ \lambda_e \phi(\theta_e^1) M_D^1 \\ \vdots \\ \lambda_e \phi(\theta_e^{2N-1}) M_D^{2N-1} \end{pmatrix}}_{\text{set D}} \quad (44)$$

In general, the limiters for different moments,  $\phi(\theta_e^0), \phi(\theta_e^1), \dots, \phi(\theta_e^{2N-1})$  are not the same. Therefore, the moment sets "U" and "D" can easily become non-realizable, leading to the non-realizable set of interpolated moments at face  $e$ . However, selecting an identical limiter, let it be  $\phi_e^{\min}$ , guarantees the realizability of the interpolated moment set  $e$ , as long as the moment sets "U" and "D" are realizable:

$$\underbrace{\begin{pmatrix} M_e^0 \\ M_e^1 \\ \vdots \\ M_e^{2N-1} \end{pmatrix}}_{\text{set } e} = (1 - \lambda_e \phi_e^{\min}) \underbrace{\begin{pmatrix} M_U^0 \\ M_U^1 \\ \vdots \\ M_U^{2N-1} \end{pmatrix}}_{\text{set U}} + \lambda_e \phi_e^{\min} \underbrace{\begin{pmatrix} M_D^0 \\ M_D^1 \\ \vdots \\ M_D^{2N-1} \end{pmatrix}}_{\text{set D}} \quad (45)$$

It is worth reiterating that the value of limiter  $\phi_e^{\min}$  is between 0 and 2. Moreover, the moment sets "U" and "D" belong to the previous time step if an explicit method is used to advance in time, and therefore they are

356 realizable.

357 It should be noted that the realizability of the interpolated moments on the  
 358 faces does not ensure the realizability of the calculated moments at the new  
 359 time step. To elaborate, let the transient term in Eq. (42) be integrated using  
 360 an explicit Euler scheme [16] and then write the fully-discretized equation  
 361 for the set of  $2N - 1$  moments:

$$\mathbf{W}_i^{n+1} = \mathbf{W}_i^n - \frac{\Delta t}{\Delta V_i} \sum_e (\mathbf{u}_e^n \cdot \hat{\mathbf{n}}_e) S_e \mathbf{W}_e^n \quad (46)$$

362 The use of an identical limiter for all the moments guarantees that the mo-  
 363 ment set  $\mathbf{W}_e^n$  be realizable, and therefore an underlying number density func-  
 364 tion ( $f_e^n$ ) can be associated to it. This allows writing Eq. (46) as:

$$f_i^{n+1} = f_i^n - \frac{\Delta t}{\Delta V_i} \sum_e (\mathbf{u}_e^n \cdot \hat{\mathbf{n}}_e) S_e f_e^n \quad (47)$$

365 The summation in the above equation can be separated into two contributions  
 366 of in-going and out-going fluxes:

$$f_i^{n+1} = f_i^n - \underbrace{\frac{\Delta t}{\Delta V_i} \sum_e \min[(\mathbf{u}_e^n \cdot \hat{\mathbf{n}}_e), 0] S_e f_e^n}_{\text{in-going fluxes}} - \underbrace{\frac{\Delta t}{\Delta V_i} \sum_e \max[(\mathbf{u}_e^n \cdot \hat{\mathbf{n}}_e), 0] S_e f_e^n}_{\text{out-going fluxes}} \quad (48)$$

367 The in-going fluxes have positive sign and cannot rise the realizability issue,  
 368 whereas, the outgoing fluxes have negative sign and can cause realizability is-  
 369 sue, i.e. negativity of  $f_i^{n+1}$ . However, the out-going fluxes can be still decom-  
 370 posed into two separate upwind and downwind contributions corresponding  
 371 to the upwind and downwind neighbouring cells of the corresponding faces.  
 372 It is noteworthy that the upwind cell of these faces indeed coincides with cell

373  $i$  since the flux at these faces is out-going. Thus, the first and third terms of  
 374 the RHS of Eq. (48) can be written as follows:

$$\begin{aligned} & \left( 1 - (1 - \lambda_e \phi_e^{\min}) \frac{\Delta t}{\Delta V_i} \sum_e \max[(\mathbf{u}_e^n \cdot \hat{\mathbf{n}}_e), 0] S_e \right) f_i^n \\ & - (1 - \lambda_e \phi_e^{\min}) \frac{\Delta t}{\Delta V_i} \sum_e \max[(\mathbf{u}_e^n \cdot \hat{\mathbf{n}}_e), 0] S_e f_{D_e}^n \end{aligned} \quad (49)$$

375 where  $f_{D_e}^n$  denotes the (downwind) neighbouring cell separated by face  $e$  from  
 376 cell  $i$ . As can be seen, the entire contribution of the cell  $i$  is positive as long  
 377 as the coefficient behind  $f_i^n$  is positive, leading to the following CFL-like  
 378 condition:

$$\frac{\Delta t}{\Delta V_i} \sum_e \max[(\mathbf{u}_e^n \cdot \hat{\mathbf{n}}_e), 0] S_e < 1 \quad (50)$$

379 Therefore, the only remaining negative contributions are due to the infor-  
 380 mation (distributions) of the downwind cells (with respect to cell  $i$ ) that  
 381 propagates back into cell  $i$ , which is the characteristic of high-order schemes.  
 382 These negative contributions can generally lead to the non-realizability issue,  
 383 i.e. negativity of  $f_i^{n+1}$ . However, similar to the previous discussion done for  
 384 one-dimensional constant-velocity cases, the negative contributions can be  
 385 kept small (in comparison to the contribution of  $f_i^n$ ) by controlling the time  
 386 step. It is noteworthy that this technique may fail as the moment sets are  
 387 near/at the boundary of the moment space, as explained before.

388 Returning back to the time-integration of the transient term in Eq. (42),  
 389 it should be noted that one notable advantage of the equal-limiter scheme  
 390 is the possibility of using implicit time-integration for the advection of the  
 391 moments. This is due the fact that the equal-limiter scheme interpolates  
 392 the moments directly, whereas, for instance, the quasi-high-order scheme is

normally implemented using explicit time-integration schemes. This aspect is particularly important when the solution of the population balance equation is incorporated into a CFD solver, since the implicit time-integration schemes are commonly adopted in these codes.

Lastly, the proposed technique is very simple from the computational point of view and can be easily implemented in three-dimensional CFD solvers. The only additional steps are comparing the limiter values calculated for the moments at each face and then replacing them with the smallest one at the corresponding face.

## 5. Numerical Examples

This section evaluates the performance of the proposed technique for the advection of moments in two different parts. The first one is focused on comparing the predictions obtained by different schemes for the advection of the moments in a mono-dimensional constant-velocity problem. The second part evaluates the performance of the schemes by solving the moment transport equations coupled with the CFD simulation of a two-dimensional transient lid-driven cavity flow.

### 5.1. One-dimensional advection with constant-velocity

This part employs the equal-limiter scheme for the advection of moments in spatially mono-dimensional problems with the disperse particle size as the only internal coordinate of the PBE. The first example deals with the pure advection of the moments without any source term, while the next examples includes the aggregation/breakage source terms in the moment transport equations. The results are compared with those obtained via a 1<sup>st</sup>-order



417 scheme and the realizable high-order scheme (or quasi-2<sup>nd</sup>-order scheme) by  
 418 Vikas et al. [6]. In addition, the analytical solution is reported whenever it  
 419 is available.

420 All the cases use 3-node quadrature to approximate the NDF. This num-  
 421 ber of nodes requires to track the first 6 moments with respect to the par-  
 422 ticle size,  $M^0, M^1, \dots, M^5$ . The calculation of the weights and abscissas of  
 423 the quadrature is done by using the Chebyshev algorithm. The spatial prob-  
 424 lems are defined over the spatial domain  $[0, 1]$ , which is discretized to cells  
 425 of identical size  $\Delta x = 0.01$ . The fluxes at the faces are calculated using  
 426 high-resolution limited-flux methods. The limiters, in turn, are computed  
 427 using the minmod function, as it was also used by Vikas et al [6]. Two ghost  
 428 cells at the left side of the domain and one ghost cell at the right side are  
 429 considered to cope with the three-cell stencil required by the high-resolution  
 430 schemes. The advection velocity,  $u$ , is set to 1.0 and  $\Delta t$  is calculated by  
 431 fixing the CFL condition equal to 0.5. The following solution procedure is  
 432 used to advance in time starting from the initial data, which is based on the  
 433 explicit fractional-step method for time integration:

- 434 1. Initialize the moments in the interior domain.
- 435 2. Apply the boundary conditions at the two left ghost cells.
- 436 3. Calculate the limiters for all the moments at each face.
- 437 4. Find the minimum limiter at each face.
- 438 5. Calculate the flux of the moments using the minimum limiter at each
- 439 face.

- 440 6. Compute the intermediate values of the moments at each interior cell  
441 using the fluxes at the corresponding left and right faces after a time  
442 step equal to  $\Delta t$ .
- 443 7. Find the weights and the abscissas of the quadrature at each interior  
444 cell using the intermediate values of the moments.
- 445 8. Calculate the source contributions at each interior cell using the corre-  
446 sponding quadrature approximation of the NDF.
- 447 9. Advance the intermediate values of the moments at each interior cell  
448 by one time step  $\Delta t$  using the calculated source terms.
- 449 10. Apply the boundary condition at the right ghost cell using zero-order  
450 extrapolation from the last interior cell of the domain.
- 451 11. Repeat steps 3 to 10 until obtaining the solution at the desired time.

452 Steps 8 and 9 (fractional-step approach) are obviously required only if the  
453 source terms are present. In this work, the source terms are treated by a  
454 single-stage method as explained in steps 8 and 9. However, these steps can  
455 be modified to use a two-stage method, leading to higher accuracy for the  
456 fractional-step approach as explained by LeVeque [15]. It should be empha-  
457 sized that this suggestion concerns the application of two-stage methods only  
458 for updating the intermediate moments by the source terms. Therefore, no  
459 realizability issue is generally expected in case of using two-stage methods  
460 instead of one-stage method only to treat the source terms, provided that  
461 the intermediate moments after the advection are realizable. Furthermore,

step 7 is done even in the case without source term to check the realizability of the moments.

More details on the problem settings are presented for each case separately.

#### 5.1.1. Pure advection of the moments

The first example is the one-dimensional pure advection of the moments, i.e. no source term, with the following initial and boundary conditions:

$$\begin{aligned} IC : \quad M^k(x_i, 0) &= \overset{\circ}{M}^k \quad \text{for } i = 0, 1, 2, \dots, p \\ BC \text{ (ghost cells)} : \quad &\begin{cases} M^k(x_{-1}, t_n) = M^k(x_{-2}, t_n) = M_b^k \\ M^k(x_{p+1}, t_n) = M^k(x_p, t_n) \end{cases} \end{aligned} \quad (51)$$

where the interior cells are numbered from 0 to  $p$ . The initial conditions  $\overset{\circ}{M}^k$  and the boundary conditions  $M_b^k$  are two sets of scaled moments having the shape of different log-normal distributions,  $\overset{\circ}{Y}$  and  $Y_b$ . The parameters of the distributions, i.e. the mean and the standard deviation of the corresponding normal distributions, are respectively  $(\overset{\circ}{\mu}, \overset{\circ}{\sigma}) = (\ln(0.008), 0.22)$  and  $(\mu_b, \sigma_b) = (\ln(0.005), 0.2)$ . Furthermore, the zero-order moments are  $\overset{\circ}{M}^0 = 20000$  and  $M_b^0 = 800000$  respectively. It should be noted that the two log-normal distributions have different parameters to avoid their quadrature approximations having the same abscissas. Otherwise, the interpolated abscissas on the faces are identical to those of the cells regardless of the employed scheme. Then, it is trivial to show that, in this special case, the quasi-2<sup>nd</sup>-order scheme proposed by Vikas et al. [6] is essentially the same as applying 2<sup>nd</sup>-order scheme directly to the moments.

Figure 2 compares the results obtained from 1<sup>st</sup>-order scheme, quasi-2<sup>nd</sup>-

483 order scheme and the proposed equal-limiter scheme. Furthermore, the an-  
 484 alytical solution is plotted in Fig. 2 to provide a benchmark. It is pointless  
 485 to report the results by the standard 2<sup>nd</sup>-order TVD scheme since, as proved  
 486 before, the corresponding results would be identical to those obtained by  
 487 the equal-limiter scheme. As expected, the solution given by the 1<sup>st</sup>-order  
 488 scheme is very diffusive. The quasi-2<sup>nd</sup>-order scheme improves the accuracy  
 489 of the results by applying 2<sup>nd</sup>-order scheme to the weights. However, the  
 490 moments do not remain bounded simply because applying a TVD scheme  
 491 to the weights does not guarantee the boundedness of the transported mo-  
 492 ments, hence appearance of the non-physical oscillations in the solutions.  
 493 The least oscillations belong to the moment of order zero as expected, since  
 494 it is simply equivalent to the sum of the weights, the variable to which the  
 495 TVD scheme is applied in the quasi-2<sup>nd</sup>-order scheme. The oscillations be-  
 496 come more obvious as the moment order increases. It should be noted that,  
 497 according to our tests, the oscillations may increase or vanish depending on  
 498 the characteristics of the underlying NDFs. The best predictions belong to  
 499 the equal-limiter scheme which is indeed the full 2<sup>nd</sup>-order TVD scheme since  
 500 this numerical example is the same as the pure advection Riemann problem  
 501 studied in Section 3. Consequently, the predictions are bounded and without  
 502 any oscillation.

### 503 5.1.2. *Moment advection with source term*

504 The next examples deal with a more practical application. The moments  
 505 of a particle size distribution are introduced and advected in the domain while  
 506 they are subject to local changes due the effect of the aggregation/breakage  
 507 of the particles. The initial and boundary conditions are the same as the case

of pure advection (see Eq. (51)). In the following, two cases are presented in which the aggregation and breakage are considered separately. Both aggregation and breakage are modeled by assuming a constant kernel. For the case of breakage, the daughter size distribution is expressed by assuming symmetric fragmentation of the particles [23]. The reasoning behind these simplistic assumptions is the possibility of obtaining analytical solutions for the moments of the NDF.

**Constant aggregation kernel.** In this case, the source term in Eq. (7) is calculated as follows [23]:

$$h_i^k = \frac{1}{2} \sum_{\alpha=1}^3 w_{i,\alpha} \sum_{\beta=1}^3 w_{i,\beta} (L_{i,\alpha}^3 + L_{i,\beta}^3)^{k/3} K_a - \sum_{\alpha=1}^3 L_{i,\alpha}^k w_{i,\alpha} \sum_{\beta=1}^3 w_{i,\beta} K_a \quad (52)$$

where  $K_a = 10^{-5} (m^3 \cdot s^{-1})$  is the aggregation kernel.

The solutions obtained by the studied schemes are shown in Fig. 3. As can be seen, both quasi-2<sup>nd</sup>-order and equal-limiter schemes improve the accuracy of the results with respect to the 1<sup>st</sup>-order scheme. It is notable that, despite employing the minimum limiter, the equal-limiter scheme produces almost comparable results to those of the quasi-2<sup>nd</sup>-order scheme. Moreover, the solutions of  $M^3$  indicate that only 1<sup>st</sup>-order and equal-limiter schemes are bounded, as expected. Instead, a slight degree of overshoot and undershoot exists in the solution of the quasi-2<sup>nd</sup>-order scheme. The appearance of these spurious oscillations is certainly due to the numerics as both aggregation and breakage of the particles have no effect on the moment of order three with respect to the particle size. Although no analytical solution is available for  $M^5$ , some degree of overshoot and undershoot can be observed visually in the solution obtained by the quasi-2<sup>nd</sup>-order scheme. Again it can be seen

that the amplitude of the oscillations are intensified as the moment order increases. It is worth mentioning that employing the standard 2<sup>nd</sup>-order TVD scheme is not feasible because the moments get corrupted shortly after starting the simulation and consequently the Chebyshev algorithm fails to calculate the weights and the abscissas required for the source calculation. Even reducing the time step by a factor of 100, equivalent to an impractically small CFL value of 0.005, cannot remedy the non-realizability problem. This shows the effectiveness of the proposed equal-limiter scheme in preserving the realizability of the moments when the 2<sup>nd</sup>-order TVD schemes are employed.

**Symmetric constant breakage kernel.** In this case, the source term in Eq. (7) is calculated as follows [23]:

$$h_i^k = \sum_{\alpha=1}^3 w_{i,\alpha} 2^{(3-k)/3} L_{i,\alpha}^k K_b - \sum_{\alpha=1}^3 w_{i,\alpha} L_{i,\alpha}^k K_b \quad (53)$$

where  $K_b = 4 \text{ (s}^{-1}\text{)}$  is the breakage kernel.

Fig. 4 depicts the results provided by the studied schemes along with the analytical solutions. The same arguments presented for the case of pure aggregation apply also to this case with the difference that here the oscillating behavior of the quasi 2<sup>nd</sup>-order scheme is more intense. This further highlights the advantage of the equal-limiter scheme whenever the boundedness of the solution is strictly required.

## 5.2. Pure advection in two-dimensional transient flow

The previous part presents satisfactory results obtained by the equal-limiter scheme in the one-dimensional constant-velocity Riemann problem examples. However, it is important to examine the predictions obtainable by the proposed scheme in systems with higher dimensions and realistic flow

fields, e.g. non-constant and/or transient velocity. For this purpose, a familiar two-dimensional transient flow, known as lid-driven cavity, is selected to compare the results for the pure advection of moments obtained by employing upwind, quasi-2<sup>nd</sup>-order and equal-limiter schemes. The moments belong to the distributions that represent the population of micro-droplets which are transported by a carrier liquid. The micro-droplets are assumed to do not have their own inertia and therefore they move with the same velocity of the carrier liquid.

The simulation domain is a square with length ( $L$ ) of 10 cm and it is discretized by a structured uniform Cartesian grid comprising of 10000 square cells of size 1 mm. The flow is confined by four boundaries of type wall, from which the top one moves with the velocity ( $U$ ) of 1 (m/s) while the others are fixed. The kinematic viscosity of the liquid ( $\nu$ ) is set to  $2.5 \times 10^{-4}$  (m<sup>2</sup>/s), which results to Reynolds number of 400 defined by  $UL/\nu$ . The liquid is assumed to be stagnant at time zero and then a transient flow develops in the liquid due to the constant velocity ( $U$ ) applied at the top wall.

The transient simulations are done by using the icoFoam solver of OpenFOAM software, which solves the governing (constant-density) Navier-Stokes equations for the liquid phase numerically by using the PISO algorithm [16]. The time step is set to 0.0001 (s) to keep the maximum Courant number below 0.1. The solution of the velocity field at three time instants are shown in Fig. 5. The solver is modified to solve simultaneously the moment transport equations. At the beginning of each time step, the moments of the micro-droplet population are advected in time using the velocity field of the previous time step. Then, the flow field of the liquid phase is updated by us-

ing the PISO algorithm. Regarding the advection of moments, as mentioned  
 in Section 4, the implicit Euler time-integration can be used with the advec-  
 tion schemes that deal with the moments directly, and therefore is adopted  
 here when the upwind and equal-limiter schemes are employed. On the other  
 hand, the quasi-2<sup>nd</sup>-order scheme is implemented with Euler explicit time-  
 integration. It should be noted that the reasoning behind employing the  
 implicit time-integration scheme is to highlight the advantage of the equal-  
 limiter scheme, which is its compatibility with the implicit approach. Con-  
 cerning the flux-limiter, the minmod function is used for the interpolation  
 of quadrature weights in case of employing quasi-2<sup>nd</sup>-order scheme and the  
 interpolation of moments in case of employing equal-limiter scheme.  
 Two different cases corresponding to two different initial conditions for the  
 moments are considered. The first initial condition is defined such that there  
 is no micro-droplets in the domain except for a square patch where a popu-  
 lation of micro droplets with average size of 100 ( $\mu\text{m}$ ) and standard devia-  
 tion of 20 ( $\mu\text{m}$ ) is introduced. The population is assumed to be distributed  
 log-normally on the size space. The initial conditions for the moments are  
 calculated based on this log-normal distribution which is scaled to adjust the  
 volume fraction of the micro-droplets equal to 0.05 (assuming spherical shape  
 for the micro-droplets). Fig. 6 depicts the initial conditions for the moment  
 of order three, along with the solutions for the same moment at  $t = 3$  s ob-  
 tained by employing the 1<sup>st</sup>-order upwind, quasi-2<sup>nd</sup>-order and equal-limiter  
 schemes. As can be seen, the solution obtained by the upwind scheme suffers  
 from high numerical diffusion. On the other hand, both the quasi-2<sup>nd</sup>-order  
 and equal-limiter schemes yield comparable results, which have higher resolu-



tion with respect to the one obtained by the upwind scheme. It is noteworthy that the same contour plots (but of different values) are obtained for the other moments, which is expected since the shape of the distribution corresponding to the underlying NDF remains the same in pure advection. As a result, the abscissas of the quadrature approximation are the same in all the cells of the domain.

As mentioned previously, the quasi-2<sup>nd</sup>-order scheme interpolates the quadrature abscissas with a 1<sup>st</sup>-order scheme, whereas it interpolates the quadrature weights with a 2<sup>nd</sup>-order scheme. Therefore, when the quadrature abscissas are the same throughout the domain, the entire resolution of the quasi-2<sup>nd</sup>-order scheme for the pure advection of moments is the same as the 2<sup>nd</sup>-order scheme. The reason is that, in this case, the value of abscissas on the faces are the same as those at the cell centers regardless of the employed scheme. Consequently, the pure advection of moments by interpolating the weights onto the faces with a given 2<sup>nd</sup>-order scheme and then constructing the moments on the faces (using the same abscissas) is equivalent to the pure advection of moments by interpolating the moments directly onto the faces using that 2<sup>nd</sup>-order scheme. However, this equivalency is not generally valid when the abscissas are not the same through the domain. Thus, it is worth examining the performance of the schemes in case of existing two different distributions, i.e. having different quadrature abscissas, in the system at time zero. For this purpose, the same square patch (with the same population of micro-droplets) defined by the initial conditions of the previous case is considered also here. However, it is assumed that another population of micro-droplet exists outside the square patch, instead of assuming no micro-droplet existing

629 in that zone. Let the population of micro-droplets out of the square patch  
 630 be also distributed log-normally on the size space with average size equal to  
 631  $50\ (\mu\text{m})$  and standard deviation of  $7.5\ (\mu\text{m})$ . This distribution is scaled to  
 632 have the volume fraction of the micro-droplets equal to 0.001. Then, the ini-  
 633 tial condition of the moments is defined based on this scaled distribution, as  
 634 shown in Figs. 7 and 8 for the moments of order zero and three respectively.  
 635 Moreover, the predictions at  $t = 3\text{ s}$  are depicted by these figures for the  
 636 mentioned moments. As can be seen in Fig. 7, the values of  $M_0$  obtained by  
 637 employing the quasi-2<sup>nd</sup>-order scheme do not remain bounded between the  
 638 limits defined by the initial conditions. It is noteworthy that in QBMM, the  
 639 transported variables are indeed the moments and therefore in the pure ad-  
 640 vection with a solenoidal velocity field, the solution for the moments should  
 641 remain bounded between the limits defined by the initial conditions. This  
 642 issue concerning the quasi-2<sup>nd</sup>-order scheme can be associated to the fact  
 643 that this scheme interpolates the weights and abscissas of the quadrature  
 644 separately, and therefore there is no guarantee that the TVD criteria [20] are  
 645 respected by this scheme. On the other hand, the solution obtained by the  
 646 equal-limiter scheme (when it is used with the minimum limiter) respects  
 647 the boundedness property of the moments. Moreover, the applied change in  
 648 the initial condition of the moments should not change the pattern of the  
 649 solution contour plots, since the current initial condition with the two dis-  
 650 tributions can be changed to a problem with initial condition similar to the  
 651 previous case (micro droplets existing only in a square patches) by a change  
 652 of variables. However, the comparison between the results shown in Fig. 8  
 653 with those depicted in Fig. 6 highlights that only the equal-limiter scheme

reproduces the same pattern for  $M_3$  in both cases. Furthermore, the pattern of the results obtained by the equal-limiter scheme for  $M_0$  and  $M_3$  shown in Figs. 7 and 8 are the same, whereas this is not the case for the results obtained by the quasi-2<sup>nd</sup>-order scheme. This final example emphasizes the advantage of employing a scheme which interpolates the moments directly, e.g. equal-limiter scheme, instead of interpolating some variables related to the moments.

## 6. Conclusions

A new technique called equal-limiter scheme was proposed to overcome the non-realizability problem that arises when the 2<sup>nd</sup>-order TVD schemes are employed to solve the moment transport equations in the context of QBMM. The central idea behind the technique is that the interpolated moments on the faces must form a realizable set when the moment fluxes are being calculated. Following this idea, it was explained that using an identical flux-limiter for all the moments at each face guarantees the realizability of the interpolated moments and consequently helps to preserve the realizability of the transported moments. Although no formal proof has been given to ensure that the equal-limiter scheme preserves the realizability of the moments under general conditions, it has been shown that this feature can be achieved in the limit of small time steps (as long as the moment sets are far from the boundary of the moment space). On the contrary, adjusting the time step can not mitigate the non-realizability problem if the limiters are independently calculated for each moment of the transported moment set. This fact was also illustrated by the numerical tests as the moments

678 did not remain realizable even with impractically small time step in the case  
 679 of employing the standard 2<sup>nd</sup>-order TVD scheme. Moreover, it was proved  
 680 that the minimum limiter is a possible practical option for the equal limiter  
 681 if the boundedness feature of the TVD schemes has to be retained. Al-  
 682 though selecting the minimum limiter may imply solutions of lower order,  
 683 the one-dimensional numerical examples showed that the results obtained by  
 684 equal-limiter and quasi-2<sup>nd</sup>-order schemes are comparable in terms of accu-  
 685 racy. More importantly, the improvement in the accuracy was observed also  
 686 for the solutions obtained by the equal-limiter scheme in a one-way coupled  
 687 QMOM-CFD simulation of a transient two-dimensional flow. Furthermore,  
 688 the new technique does not only improve the accuracy of the solution with  
 689 respect to the 1<sup>st</sup>-order solution but also keeps the solution bounded, which  
 690 was shown to be an advantage over the quasi-2<sup>nd</sup>-order scheme by comparing  
 691 their predictions in both one- and two-dimensional numerical examples. In  
 692 addition, the implementation of the scheme is simple and can be integrated  
 693 into the CFD simulations easily.

694 The future works will focus on applying the proposed scheme to the  
 695 three-dimensional CFD simulation of polydisperse systems and studying its  
 696 predictions in comparison to those of the other discretization schemes.

## 697 References

- 698 [1] D. L. Marchisio, R. O. Fox, Computational Models for Polydisperse  
699 Particulate and Multiphase Systems, Cambridge Series in Chemical En-  
700 gineering, Cambridge University Press, Cambridge, UK, 2013.
- 701 [2] R. G. Gordon, Error bounds in equilibrium statistical mechanics, Jour-  
702 nal of Mathematical Physics 9 (1968) 655–663.
- 703 [3] J. C. Wheeler, Modified moments and Gaussian quadratures, Rocky  
704 Mountain Journal of Mathematics 4 (1974) 287–296.
- 705 [4] O. Desjardins, R. O. Fox, P. Villedieu, A quadrature-based moment  
706 method for dilute fluid-particle flows, Journal of Computational Physics  
707 227 (2008) 2514–2539.
- 708 [5] D. L. Wright Jr., Numerical advection of moments of the particle size  
709 distribution in Eulerian models, Journal of Aerosol Science 38 (2007)  
710 352–369.
- 711 [6] V. Vikas, Z. J. Wang, A. Passalacqua, R. O. Fox, Realizable high-order  
712 finite-volume schemes for quadrature-based moment methods, Journal  
713 of Computational Physics 230 (2011) 5328–5352.
- 714 [7] A. Buffo, M. Vanni, D. L. Marchisio, On the implementation of mo-  
715 ment transport equations in openfoam: boundedness and realizability,  
716 International Journal of Multiphase Flow 85 (2016) 223–235.
- 717 [8] D. Kah, F. Laurent, M. Massot, S. Jay, A high order moment method

- 718       simulating evaporation and advection of a polydisperse liquid spray,  
719       Journal of Computational Physics 231 (2) (2012) 394–422.
- 720       [9] F. Laurent, T. T. Nguyen, Realizable second-order finite-volume  
721       schemes for the advection of moment sets of the particle size distri-  
722       bution, Journal of Computational Physics 337 (2017) 309–338.
- 723       [10] C. Berthon, et al., Stability of the MUSCL schemes for the Euler equa-  
724       tions, Communications in Mathematical Sciences 3 (2) (2005) 133–157.
- 725       [11] D. Ramkrishna, Population Balances: Theory and Applications to Par-  
726       ticulate Systems in Engineering, 1<sup>st</sup> Edition, Academic Press, 2000.
- 727       [12] D. L. Marchisio, R. O. Fox, Solution of population balance equations  
728       using the direct quadrature method of moments, Journal of Aerosol  
729       Science 36 (2005) 43–73.
- 730       [13] J. A. Shohat, J. D. Tamarkin, The problem of moments, American  
731       Mathematical Society, New York, USA, 1943.
- 732       [14] M. Pigou, J. Morchain, P. Fede, M.-I. Penet, G. Laronze, New develop-  
733       ments of the extended quadrature method of moments to solve popu-  
734       lation balance equations, Journal of Computational Physics 365 (2018)  
735       243–268.
- 736       [15] R. J. LeVeque, Finite Volume Methods for Hyperbolic Problems, 1<sup>st</sup>  
737       Edition, Cambridge University Press, 2002.
- 738       [16] J. H. Ferziger, M. Peric, Computational Methods for Fluid Dynamics,  
739       3<sup>rd</sup> Edition, Springer, Berlin, Germany, 2001.

- 740 [17] P. Roe, M. Baines, Algorithms for advection and shock problems, in:  
741 Numerical Methods in Fluid Mechanics, 1982, pp. 281–290.
- 742 [18] B. Van Leer, Towards the ultimate conservative difference scheme. II.  
743 monotonicity and conservation combined in a second-order scheme,  
744 Journal of computational physics 14 (4) (1974) 361–370.
- 745 [19] C. Yuan, R. O. Fox, Conditional quadrature method of moments for  
746 kinetic equations, Journal of Computational Physics 230 (2011) 8216–  
747 8246.
- 748 [20] A. Harten, High resolution schemes for hyperbolic conservation laws,  
749 Journal of computational physics 49 (3) (1983) 357–393.
- 750 [21] P. K. Sweby, High resolution schemes using flux limiters for hyperbolic  
751 conservation laws, SIAM journal on numerical analysis 21 (5) (1984)  
752 995–1011.
- 753 [22] H. K. Versteeg, W. Malalasekera, An Introduction to Computational  
754 Fluid Dynamics: The Finite Volume Method, 2<sup>nd</sup> Edition, Pearson Ed-  
755 ucation, 2007.
- 756 [23] D. L. Marchisio, R. D. Vigil, R. O. Fox, Quadrature method of moments  
757 for aggregation-breakage processes, Journal of Colloid and Interface Sci-  
758 ence 258 (2003) 322–334.

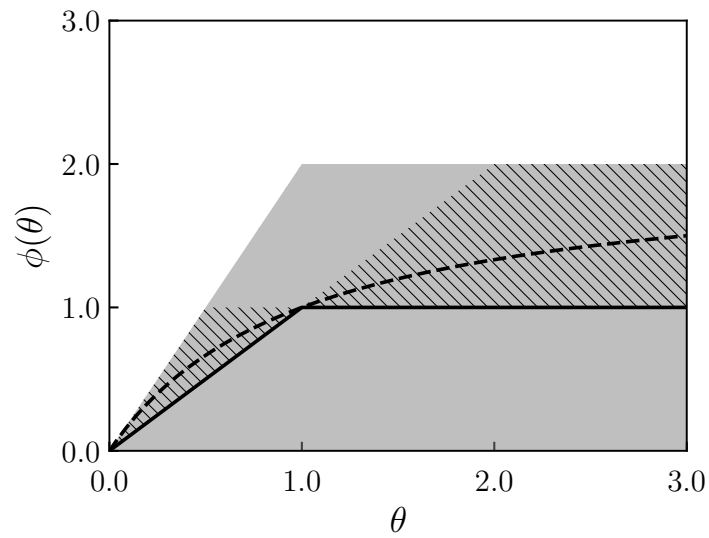


Figure 1: Flux-limiter functions. The shaded area specifies the TVD region and the hatched area is the 2<sup>nd</sup>-order region by Sweby [21]. The minmod [17] and van Leer [18] limiter functions are shown by the continuous and dashed curves respectively.



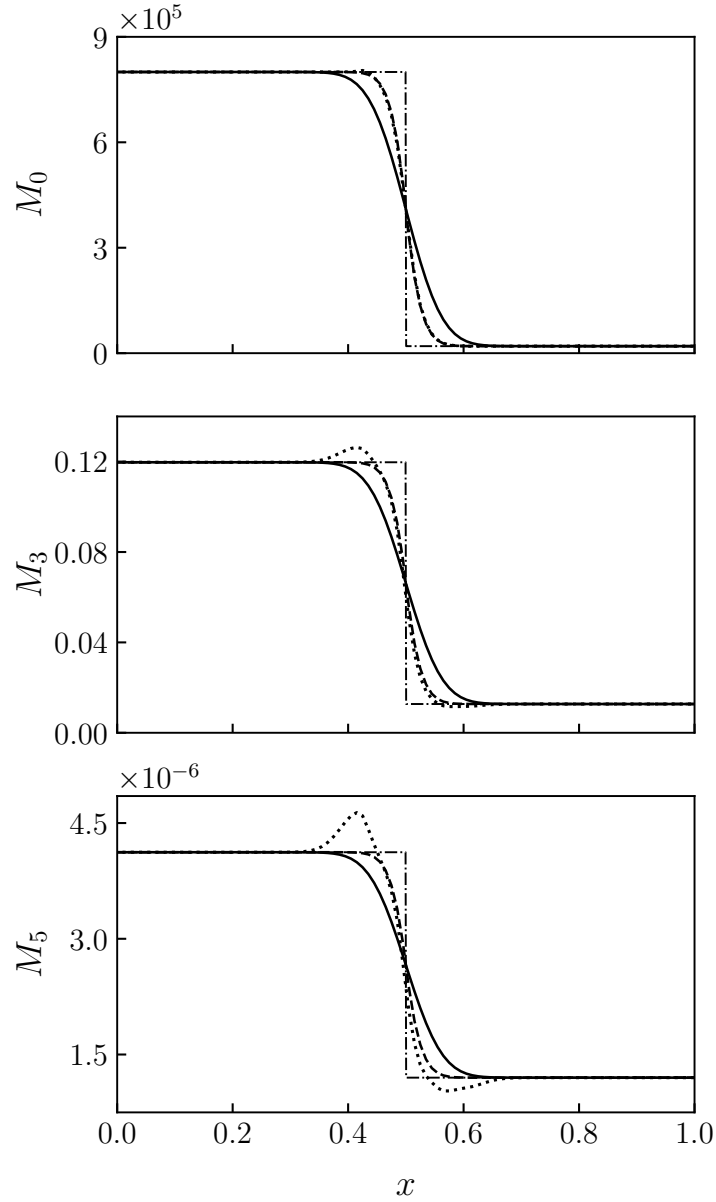


Figure 2: Comparison of the results obtained by employing different schemes for the case of pure advection: 1) analytical solution (dot-dashed line); 2) upwind scheme (continuous line); 3) quasi 2<sup>nd</sup>-order scheme (dotted line); 4) equal-limiter scheme (dashed line)

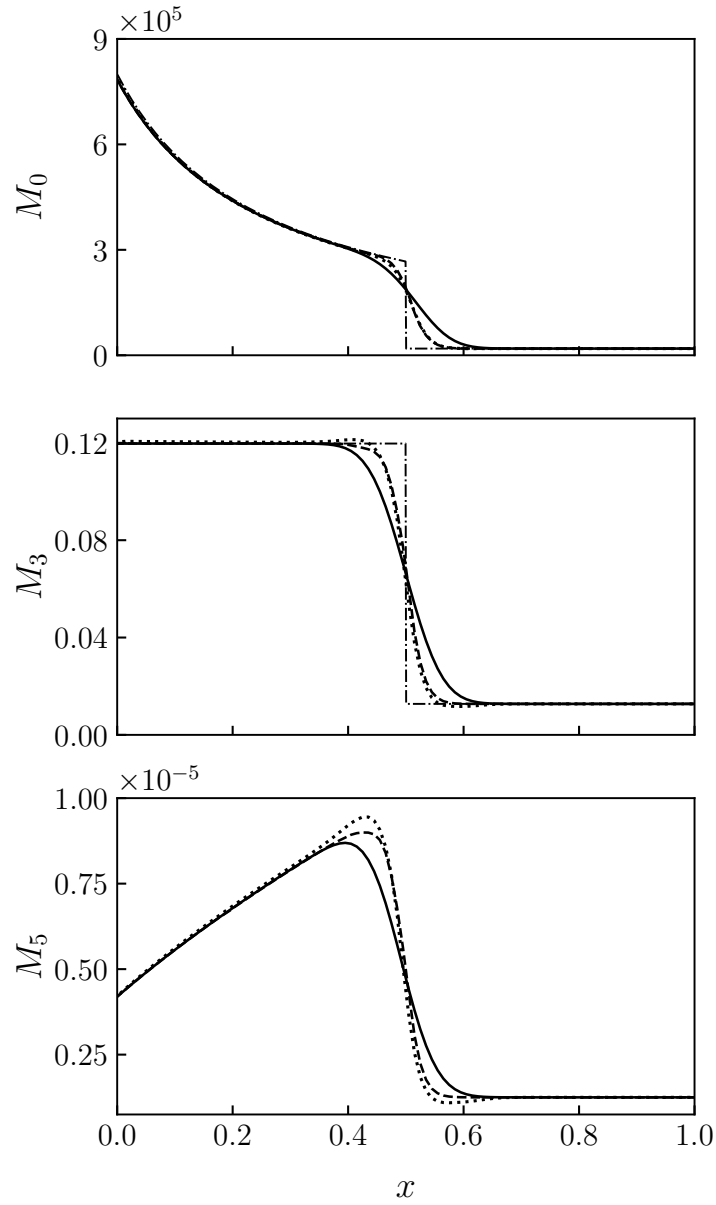


Figure 3: Comparison of the results obtained by employing different schemes for the case of constant aggregation kernel: 1) analytical solution if available (dot-dashed line); 2) upwind scheme (continuous line); 3) quasi 2<sup>nd</sup>-order scheme (dotted line); 4) equal-limiter scheme (dashed line)

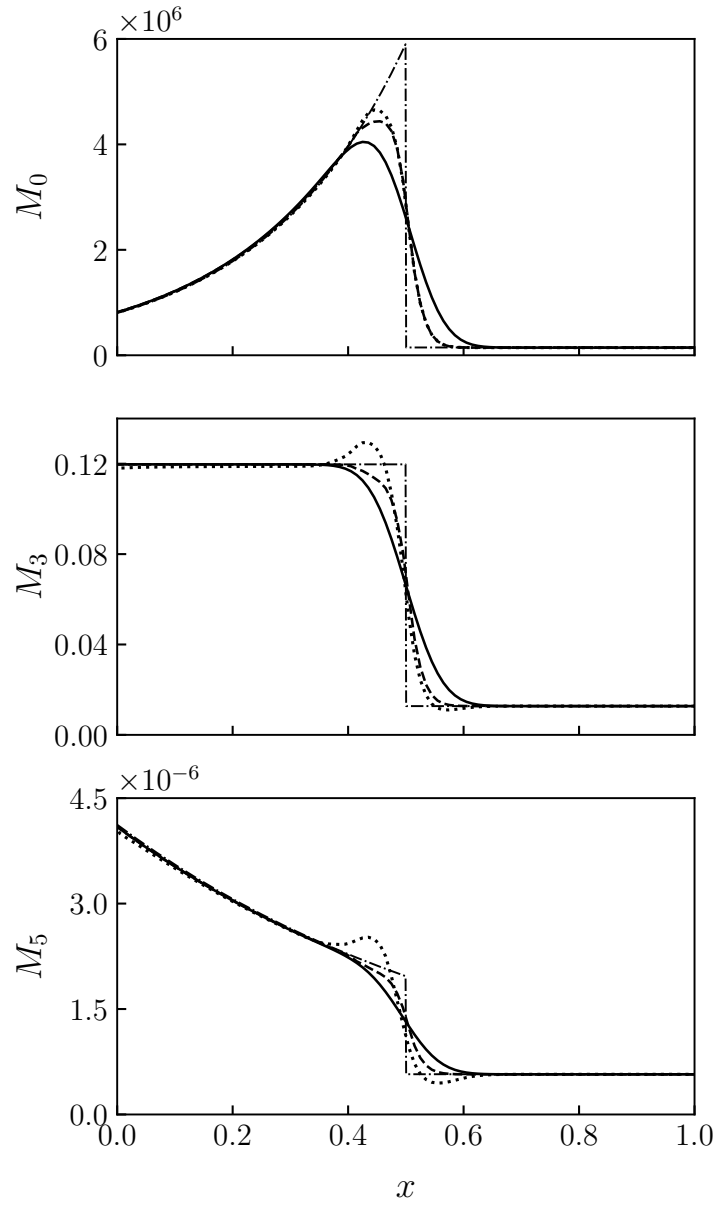


Figure 4: Comparison of the results obtained by employing different schemes for the case of symmetric constant breakage kernel: 1) analytical solution (dot-dashed line); 2) upwind scheme (continuous line); 3) quasi 2<sup>nd</sup>-order scheme (dotted line); 4) equal-limiter scheme (dashed line)

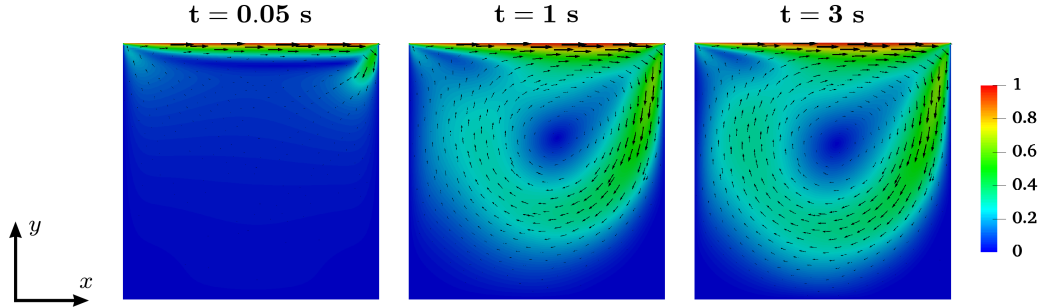


Figure 5: Velocity field (m/s) of the simulated 2-D lid-driven cavity flow at three time instants.

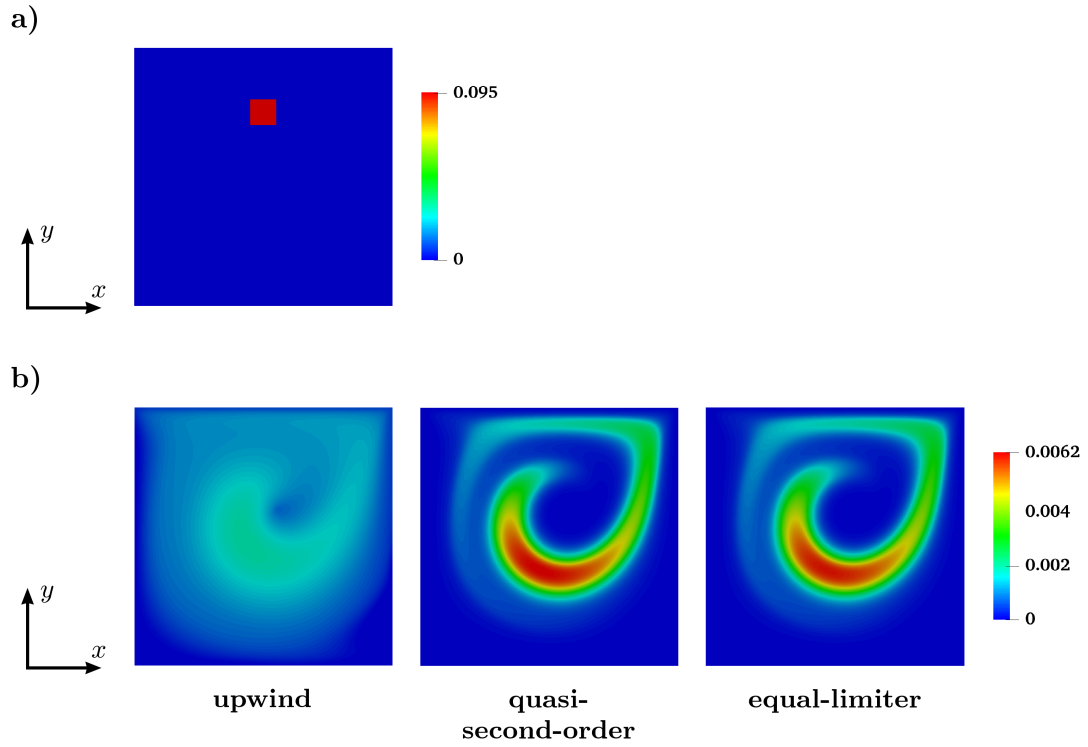


Figure 6: Comparison of the studied schemes for the advection of  $M_3$  in the 2-D cavity flow. (a) The initial condition at  $t = 0$ ; (b) the predictions obtained by employing the different schemes at  $t = 3$ .

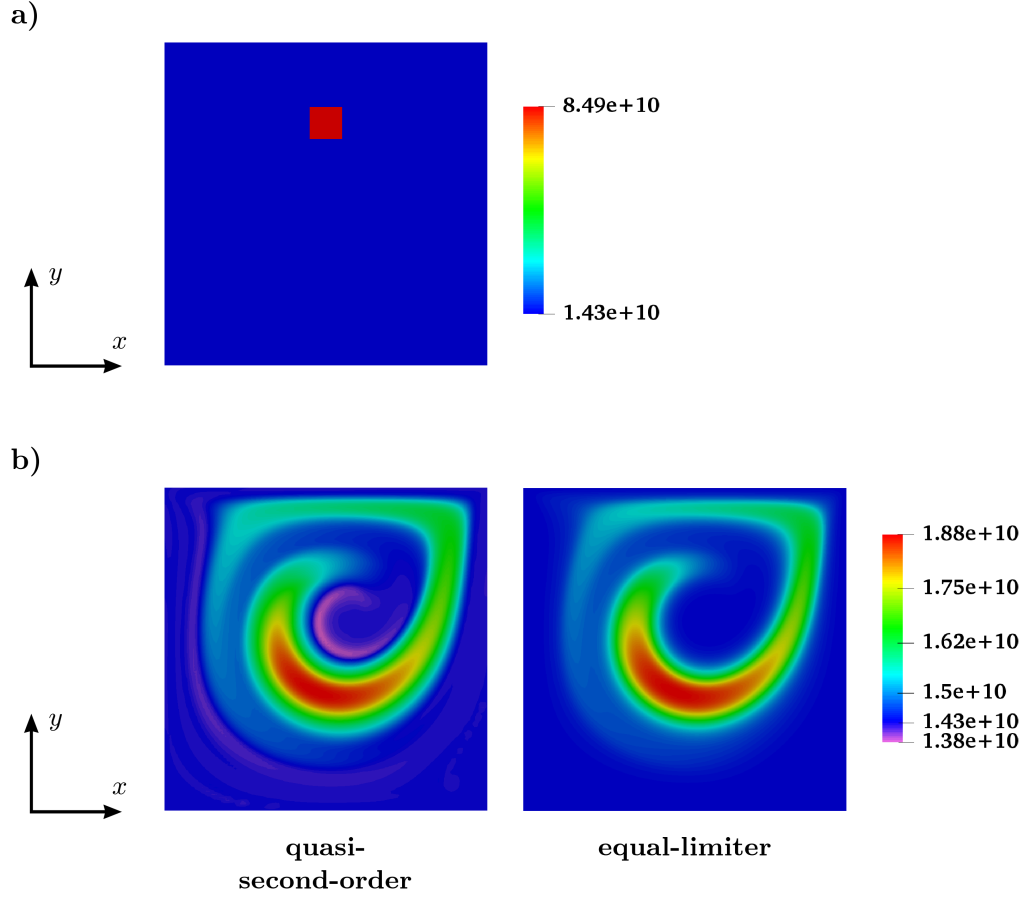


Figure 7: Comparison of the studied schemes for the advection of  $M_0$  in the 2-D cavity flow in case of existing two different distributions in the domain. (a) The initial condition at  $t = 0$ ; (b) the predictions obtained by employing the different schemes at  $t = 3$ .

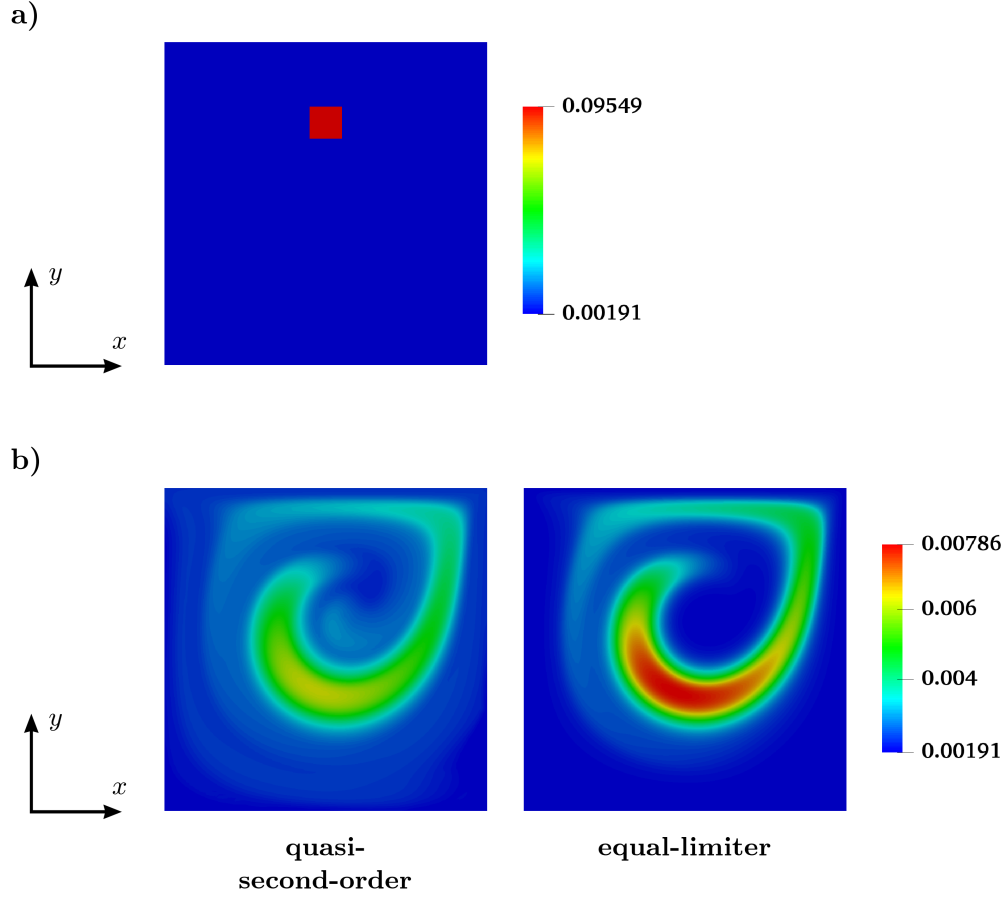


Figure 8: comparison of the studied schemes for the advection of  $M_3$  in the 2-D cavity flow in case of existing two different distributions in the domain. (a) The initial condition at  $t = 0$ ; (b) the predictions obtained by employing the different schemes at  $t = 3$ .